ASM Sc. J., 18, 2023

https://doi.org/10.32802/asmscj.2023.1432

Effects of Solution pH on Chemical Bath Deposited Iron-Sulfide-Oxide with Tartaric Acid Presence

M.H. Amri[1], A.A. Ariff[1], A. Supee[1,2*] and M.Z. Mohd Yusop[3]

[1]*Faculty of Chemical and Energy Engineering, Universiti Teknologi Malaysia, 81310 Johor Bahru, Johor, Malaysia*

[2]*Energy Management Group, Faculty of Chemical and Energy Engineering, Universiti Teknologi Malaysia, 81310 Johor Bahru, Johor, Malaysia*

[3]*Faculty of Mechanical Engineering, Universiti Teknologi Malaysia, 81310 Johor Bahru, Johor, Malaysia*

A chemical bath deposition (CBD) contained sodium thiosulfate ($Na_2S_2O_3$), iron (II) sulfate heptahydrate ($FeSO_4.7H_2O$), and L(+)-tartaric acid ($C_4H_6O_6$) as the complexing agent has been used to deposit the iron-sulfide-oxide (FeS_xO_y) films. The effects of different solution pH (5.0-9.0) on film properties were investigated. The thicknesses of the film analysed from the cross-sectional images of Scanning Electron Microscopy (SEM) showed the thickness of the film is increasing with increasing pH. The X-Ray Diffraction (XRD) pattern and the hot probe method revealed that all the deposited films are crystalline, and possess n-type semiconductor behaviour due to high oxygen content (around 72-82%). Larger crystallite sizes with extra peaks of goethite and hematite were present for the films with pH > 7.0, while, better film uniformity and grains distribution, as well as clear absorption edge in transmittance measurement, were obtained for the film with pH 5.0.

Keywords: FeS_xO_y; chemical bath deposition; tartaric acid; solution pH; uniformity

I. INTRODUCTION

Iron sulfide (pyrite-FeS_2) is an attractive solar cell material since its elements are abundant (5.63%) in Earth's crust, non-toxic, and its material extraction cost (~$0.03/kg) is 57 times lower as compared to silicon (~$1.70/kg) makes it far better in terms cost-effectiveness as compared to silicon (Srivastava & Ingole, 2020). For the performance, a 4% efficiency of pyrite solar cell obtained with a material consumption of 0.3 kg/m^2 can result in equivalent output as 19% efficiency of a silicon solar cell produced by 1 kg/m^2 material consumption (Rahman *et al.*, 2020). Besides, FeS_2 has a high optical absorption coefficient ($\alpha > 10^5$ cm^{-1}) for $\lambda \leq 700$ nm (Henríquez *et al.*, 2016; Qin *et al.*, 2018) and could display the n- (Walter *et al.*, 2017; Srivastava *et al.*, 2017) or p- type (Supee & Ichimura, 2016; Bhandari *et al.*, 2015) semiconductor behaviour (n: excess of the electron; p: excess of the hole) depending on impurity (oxygen) inclusion. FeS_2 is suitably applied as an alternative material for absorber (p-type) or window layer (n-type) in solar cells due to the above-mentioned properties.

So far, various methods have been used to deposit FeS_2 thin films including spray pyrolysis (Orletskii *et al.*, 2016), electrochemical deposition (ECD) (Prabukanthan *et. al.*, 2017; Kawai *et al.*, 2014), sulfurization of iron films (Adusumilli *et al.*, 2016), chemical bath deposition (CBD) (Aluri *et al.*, 2015; Vedavathi *et al.*, 2015; Kassim *et al.*, 2012), sol-gel deposition (Kment *et al.*, 2014), and others. In the CBD method, the aqueous solution used consists of ions for the targeted material of the thin film (Kassim *et al.*, 2010; Manikandan *et al.*, 2014), and the complexing agents are generally added to improve the solution stability, prevent metal hydroxide precipitation, produce sufficient adherence or smooth microstructures. The effects of complexing agents on the iron sulfide-based film properties could be found in works explained by previous scholars (Supee & Ichimura,

*Corresponding author's e-mail: aizuddin@utm.my

2016; Vedavathi *et al.*, 2015; Kassim *et al.*, 2012; Manikandan *et al.*, 2014; Hidzi *et al.*, 2019; Hidzir *et al.*, 2021).

The status quo exhibited that the power conversion efficiency (PCE) of FeS_2-based solar cells is still low (≤ 3%) (Luo *et al.*, 2015) and far behind the theoretical value (20%) (Ennaoui *et al.*, 1985). Many efforts have been made to boost the existing efficiency, which focuses on the heterostructures formation (different combinations of n- and p- type materials) (Wang *et al.*, 2012; Kawai *et al.*, 2016; Supee & Ichimura, 2017), yet, still unsuccessful. This is due to the poor quality of interface/bulk single film, which consequently results in low-efficiency solar cells. Previously, we found a significant improvement in bulk single iron sulfide film properties with the addition of 50 mM tartaric acid as the complexing agent (Supee & Ichimura, 2016; Hidzi *et al.*, 2019; Hidzir *et al.*, 2021). The film is named iron-sulfide-oxide (FeS_xO_y) because of the oxygen inclusion present.

In this work, we extend our previous work of CBD FeS_xO_y films with 50 mM L(+)-tartaric acid ($C_4H_6O_6$) as the complexing agent (Hidzi *et. al.*, 2019; Hidzir *et al.*, 2021) by examining the effects of solution pH (5.0, 7.0, 8.0, 9.0) on the properties of deposited films. To the best of our knowledge, most scholars deposited the iron sulfide-based film at a solution pH ≤ 5.0 (acidic condition) (Kassim *et al.*, 2010; Annuar *et al.*, 2009; Akhtar *et al.*, 2015; Botchway *et al.*, 2019), and no published works are using the pH > 5.0. It should be noted that, from the viewpoint of fabricating a good iron sulfide-based solar cell with FeS_xO_y as the window/absorber layers, it is valuable to investigate the effects of solution pH (acidic, neutral, and alkaline conditions) towards properties of single bulk deposited film.

II. MATERIALS AND METHOD

All the chemicals used in Table 1 were purchased from Kanto Electronic Chemicals (M) Sdn. Bhd., and used as it is without further purification. Those chemicals were mixed in a beaker containing 50 ml of de-ionised water (DI). The fluorine-tin-oxide (FTO)-coated glass substrate is used as per received from the Latech Scientific Supply Pte. Ltd. (dimension: 10 mm x 25 mm; resistivity value = 7 Ωcm^{-2}). Before each deposition of FeS_xO_y thin film, the FTO substrate was ultrasonically cleaned using alkyl benzene (C_6H_6), and acetone (CH_3COCH_3), and rinsed with DI water. The FTO was masked using heat-resistant masking tape for the targeted deposition area (10 mm x 10 mm) on the FTO surface. In CBD, the total deposition time and the temperature were set to 3 h and 75 °C, respectively. To determine the effects of solution pH on FeS_xO_y film properties, the addition of NH_3 (diluted NH_3 in DI) was adjusted to desired pH value. In our preliminary works, we tried the solution pH of 3.0 obtained by the addition of sulphuric acid (H_2SO_4), however, we observed a white cloudy solution appearance before the deposition. Furthermore, yellow precipitation was observed at the bottom of the beaker after the deposition process was completed. Therefore, we exclude the pH of 3.0 and only consider the pH with no precipitation in the solution (pH 5.0, 7.0, 8.0, 9.0). A magnetic stirrer with 100 revolutions per minute (RPM) was used throughout the deposition to ensure the solution used is in perfect mixing condition. After the completion of the CBD process, the FTO substrate (with FeS_xO_y film deposited on it) was carefully removed from the solution, followed by removing the heat-resistant masking tape using a tweezer and then fully dried using a dryer before being stored in vacuum storage.

Table 1. Related chemical information

No.	Chemical name (chemical formula)	Formula weight (FW) gM^{-1}	Concentration (mM)/amount
1	Sodium thiosulfate ($Na_2S_2O_3$)	158.11	100
2	Iron (II) sulfate heptahydrate ($FeSO_4.7H_2O$)	278.01	30
3	L(+)-tartaric acid ($C_4H_6O_6$)	150.09	50
4	Ammonia solution (NH_3)	17.03	As required for desired pH adjustment

Surface morphology, thickness, and compositional analysis were performed using Scanning Electron Microscopy (SEM) equipped with Energy Dispersive X-Ray Spectroscopy (EDX): SEM iT300LV (Jeol). X-ray diffraction patterns were recorded by SmartLab X-ray Diffractometer (Rigaku) with CuKα as the radiation source. Raman spectra were measured using Raman Xplora Plus (Horiba Scientific) with near-

infrared (IR) 785 nm laser wavelength as an excitation source. Optical transmittance was measured using UV-1800 UV–Vis Spectrophotometer (Shimadzu Scientific Instruments Inc.). A hot probe method was used to determine the semiconductor behaviour whereby a couple of hot and cold probes were attached to the deposited films. The hot probe was connected to the multimeter's positive (+) terminal while the cold probe was connected to the negative (-) terminal. For p-type semiconductor behaviour, the multimeter (under-voltage mode) pointer will be deflected in a negative direction, and vice versa for n-type semiconductor behaviour (Axelevitch & Golan, 2013). A Scherrer equation shown in Equation (1) was used to calculate an average crystallite size for the deposited films (Patterson, 1939):

$$d = \frac{k\lambda}{\beta \cos \theta} \quad (1)$$

whereby

d = average crystallite size-in nm

k = dimensionless shape factor (typical value is about 0.94)

λ = x-ray wavelength (typical value for CuKα is about 0.154056 nm)

β = line broadening at half the maximum intensity (full width at half maximum-FWHM)-in radians

θ = Bragg angle or peak position-in radians

III. RESULTS AND DISCUSSION

The effects of solution pH (5.0, 7.0, 8.0, 9.0) on the surface morphology of FeS_xO_y films as well as the film thicknesses are shown in Figure 1. In Figure 1, the left image represents the surface morphology while the right image illustrates the thickness of the films. The thickness of the deposited films was increased from 514.75 nm to 823.59 nm when the pH of the solution was increased from 5.0 (Figure 1(a)-right image) to 9.0 (Figure 1(d)-right image). Besides, the film deposited under pH 5.0 (Figure 1(a)-left image) has shown better quality in terms of uniformity and grain distribution. The small-flower-like grains were formed (Figure 1(b)-left image) when the pH is increased to 7.0. Further increment in pH to 9.0 has resulted in a larger size of flower-like/agglomeration grains.

The results of an elemental compositional analysis performed by EDX are depicted in Figure 2. Overall, high oxygen (O) content (around 72-82%) was observed, and low iron (Fe) and sulfur (S) contents (< 20%) were obtained regardless of solution pH. The solution pH of 8.0 exhibits the turning point for the decreasing trend of oxygen content and the increasing trend of sulfur and iron contents.

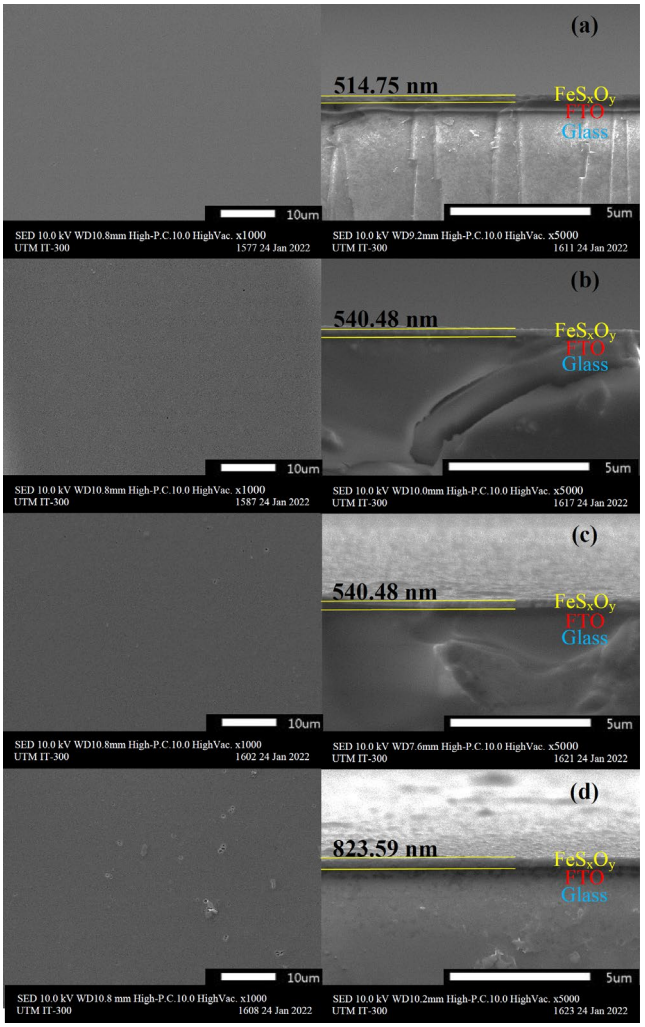

Figure 1. Left: surface morphology (x 1000), and right: cross-sectional images (x 5000) for the FeS_xO_y films deposited at different solution pH of (a) 5.0, (b) 7.0, (c) 8.0, and (d) 9.0

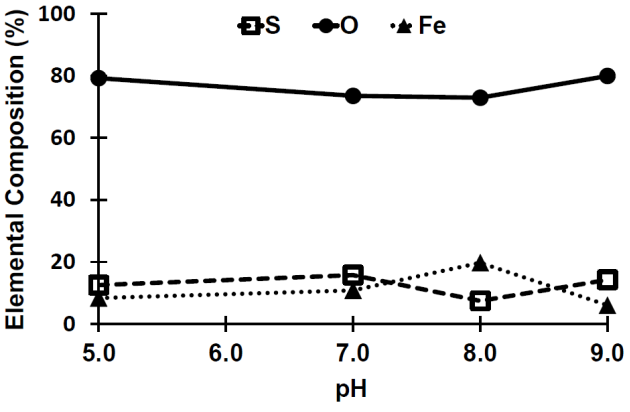

Figure 2. Elemental compositional analysis by EDX

Figure 3 illustrates the XRD patterns for FTO-coated glass substrates and FeS_xO_y films deposited at different solution pH. JCPDS 29-0713 (orthorhombic goethite-αFeOOH), JCPDS 1309-37-1 (hexagonal hematite-αFe_2O_3), and JCPDS 42-1340 (cubic pyrite-FeS_2) which is consistent with the conclusion reported in previous works (Wu *et al.*, 2021; Nie *et al.*, 2019; Saragi *et al.*, 2018) has been used for peaks identification. There was no peak observed in Figure 3(a) which reflects that the FTO substrate is amorphous. For the pH higher than 7.0 (pH 8.0-Figure 3(d), and 9.0-Figure 3(e)), there are two additional peaks appeared named goethite which is located at 2θ = 26.66˚-plane (120), and hematite which is located at 2θ = 54.76˚-plane (116). The remaining peaks of hematite: 2θ = 33.85˚-plane (104), pyrite: 2θ = 37.88˚-plane (210), and goethite: 2θ = 51.75˚-plane (221) were present in all the deposited films regardless of pH.

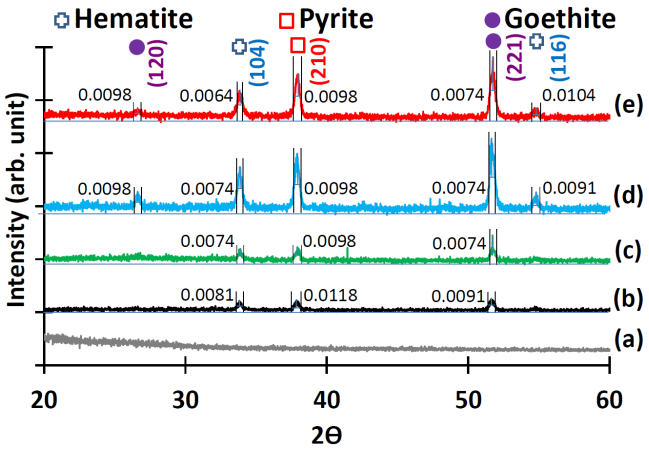

Figure 3. X-ray diffraction pattern of (a) FTO substrate, FeS_xO_y deposited at solution pH of (b) 5.0, (c) 7.0, (d) 8.0, and (e) 9.0

Based on Figure 3, it seems that a narrow/smaller peak width (FWHM) was obtained with increasing pH. It shows that the films deposited with higher pH possess higher crystallinity (larger crystallite size) as compared to lower pH. These qualitative findings were further confirmed by using a quantitative method whereby a Scherrer equation was used for average crystallite size calculation. The estimation of β and its value (numbers that use the black font colour) are displayed in Figure 3. For a better illustration, the input used in a Scherrer equation, as well as the average crystallite size, were listed in Table 2. Under pH 9.0, a larger crystallite size of 23.7 nm (2θ = 33.85˚-plane (104)) was obtained, and this exactly corresponds to the visual observation (qualitative) in Figure 3.

In published works (Hidzi *et al.*, 2019; Hidzir *et al.*, 2021), we have explained the influence of complexing agent (L(+)-tartaric acid with different concentrations) on FeS_xO_y film properties, the transformation of pyrite to hematite, as well as the iron oxide (hematite) suppression by the 50 mM L(+)-tartaric acid. In this work, we found similar effects whereby the solution pH ≤ 7.0 produced less goethite (absence of a peak at 2θ = 26.66˚-plane (120)) and hematite (absence of a peak at 2θ = 54.76˚-plane (116)) peaks. Thus, it is concluded that the solution pH ≤ 7.0 can delay the transformation of FeS_xO_y to hematite.

Table 2. Input used in a Scherrer equation (extracted from Figure 3) and calculated average crystallite size

pH	Line broadening at half the maximum intensity (full width at half maximum-FWHM) - β (radians)	Bragg angle or peak position - θ (degree)	Bragg angle or peak position - θ (radians)	Average crystallite size - d (nm)
8.0	0.0098	26.66	0.4654	15.2
9.0	0.0098			15.2
5.0	0.0081	33.85	0.5909	18.7
7.0	0.0074			20.4
8.0	0.0074			20.4
9.0	0.0064			23.7
5.0	0.0118	37.88	0.6612	13.0
7.0	0.0098			15.7
8.0	0.0098			15.7
9.0	0.0098			15.7
5.0	0.0091	51.75	0.9033	17.7
7.0	0.0074			21.7
8.0	0.0074			21.7
9.0	0.0074			21.7
8.0	0.0091	54.76	0.9559	17.9
9.0	0.0104			15.6

Figure 4 displays the Raman spectra for the films deposited at different solution pH. In previously published works, Raman peaks related to iron sulfide/iron oxide are as follows: pyrite (FeS_2): 336, 373 cm^{-1} (Morrish *et al.*, 2012); marcasite (FeS_2): 319, 324, 382 cm^{-1} (Morrish *et al.*, 2012); pyrrhotite ($Fe_{1-x}S$): 152, 292, 354 cm^{-1} (Bi *et al.*, 2011); iron-sulfide-oxide (FeS_xO_y): 249, 305 cm^{-1} (Umehara *et al.*, 2012); goethite (αFeOOH): 298, 397, 414, 474, 550 cm^{-1} (Thibeau *et al.*, 1978), and hematite (αFe_2O_3): 217, 285, 397 cm^{-1} (Morrish *et al.*, 2012). In this work, all the deposited films showed the $Fe_{1-x}S$, hematite, and goethite peaks which are located at the wavelength around 152, 218, and 473 cm^{-1}, respectively.

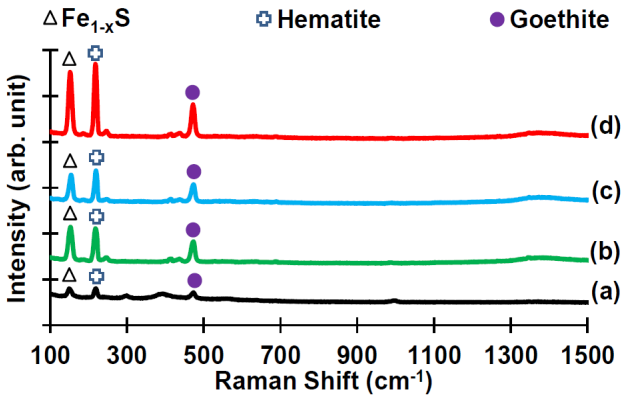

Figure 4. Raman spectra of FeS_xO_y films at different solution pH of (a) 5.0 (b) 7.0, (c) 8.0, and (d) 9.0

The measured optical transmittance is depicted in Figure 5. Overall, all the deposited films exhibited a comparable optical transmittance, nonetheless, only the film deposited at a solution pH of 5.0 shows a clear absorption edge in the visible wavelength range (around 400-500 nm).

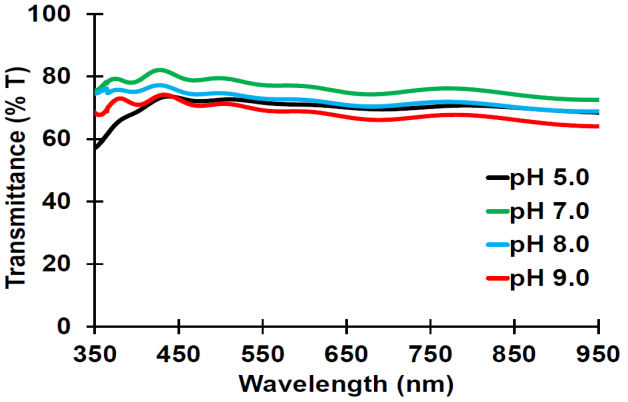

Figure 5. Transmittance for the deposited FeS_xO_y films at different solution pH of (a) 5.0 (b) 7.0, (c) 8.0, and (d) 9.0

The Tauc's plot (indirect bandgap: $(\alpha h\nu)^{1/2}$ vs. hν; direct bandgap: $(\alpha h\nu)^2$ vs. hν) was used to estimate the bandgap of the film with a clear absorption edge (pH 5.0), whereby α is the absorption coefficient and hν is the photon energy. The plot of $(\alpha h\nu)^{1/2}$ vs. hν in Figure 6(a) does not have a clear linear portion, while in the plot of $(\alpha h\nu)^2$ vs. hν portrayed in Figure 6(b), extrapolations of the linear part would intersect the x-axis at about 3.21 eV. The bandgap for the iron sulfide/oxide-based films are reported as followed: marcasite (FeS_2): < 0.30 eV (Nakamura & Yamamoto, 2001); pyrite (FeS_2): 0.95 eV (Ferrer *et al.*, 1990); pyrrhotite ($Fe_{1-x}S$): 0.2 eV (Henríquez *et al.*, 2016); goethite (αFeOOH): 2.5-3.1 eV (Zhang *et al.*, 2011); and hematite (αFe_2O_3): 1.87 Ev (Akhtar *et al.*, 2015). The estimated bandgap for the film with the solution pH of 5.0 is 3.21 eV, obviously greater than goethite (αFeOOH) and hematite (αFe_2O_3).

To this point, there are no published works for the FeS_xO_y films with such a large bandgap. Presently, we cannot describe why that film possesses such a large bandgap despite the fact the hematite (αFe_2O_3)-218 cm^{-1} is the dominance peak in the Raman result (Figure 4), and goethite (αFeOOH)-$2\theta = 51.75^\circ$-plane (221) is the dominance peak in XRD measurement (Figure 3). The visual appearance of the solution before the deposition is almost clear and no precipitation is found in the bath solution throughout/after the deposition process. For the deposited film, the visual appearance is almost transparent. Yet, the absorption edge in the visible wavelength range (around 400-500 nm) as illustrated in Figure 5 is still clear. Based on Raman spectra in Figure 4, there is no peak for the FTO-coated glass substrate-1090 cm^{-1} (La *et al.*, 2012) appeared, and referring to the surface morphology in Figure 1, better quality of the film in terms of uniformity and grains distribution has been obtained. Our EDX results in Figure 2 for all the films including the film deposited under pH 5.0 contained high oxygen (O) content (about 72-82%). Hence, the oxygen content appears to have a strong influence on the film properties, but the mechanism is not understood. For the hot probe measurement, all the deposited films revealed n-type semiconductor behaviour regardless of solution pH, which reflects their application as window layer material in solar cell applications.

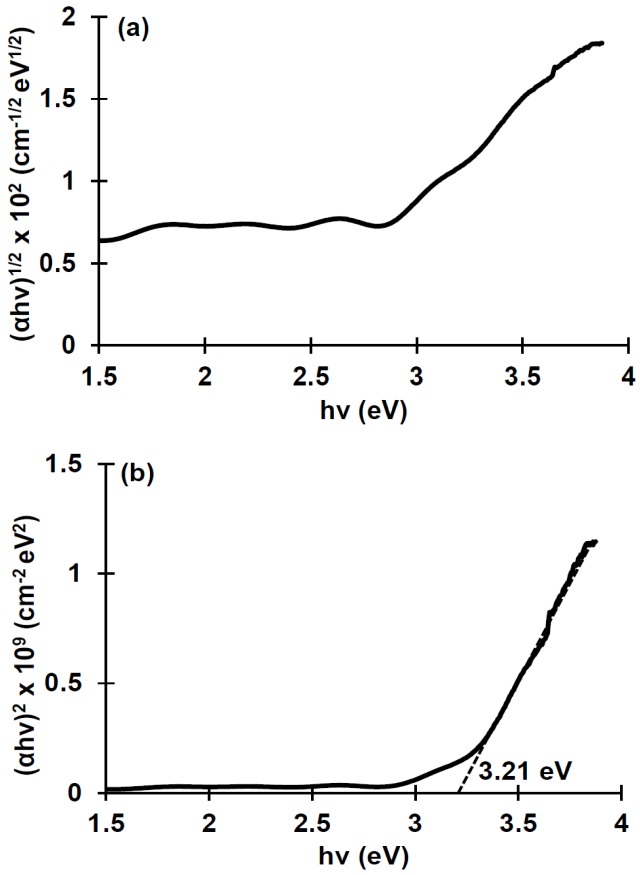

Figure 6. Plots of (a) $(\alpha h\nu)^{1/2}$, and (b) $(\alpha h\nu)^2$ vs. hν for the film deposited at a solution pH of 5.0

IV. CONCLUSION

Iron-sulfide-oxide (FeS_xO_y) films were deposited on FTO-coated glass substrates via a CBD method at different solution pH which ranged from acidic to alkaline conditions (pH: 5.0, 7.0, 8.0, 9.0), for 3 h at 75 °C from an aqueous solution containing 50 mM $C_4H_6O_6$, 100 mM $Na_2S_2O_3$, and 30 mM $FeSO_4.7H_2O$. The crystallite size increased with increasing solution pH. Better film uniformity and clear absorption edge were obtained for the film produced by the solution pH of 5.0. Furthermore, the hematite formation was delayed for the solution pH ≥ 7.0. All the films exhibited n-type semiconductor behaviour. In the future, we will examine the effects of sulfur annealing temperature on the transformation of n- to p- type of FeS_xO_y films using a solution pH of 5.0, so that, the fabrication of homostructure solar cells using iron sulfide as the base material in both the window and absorber layers could be realised. This pH selection is due to the interface quality enhancement factor that could be obtained which consequently could lead to improvements in the performance of solar cells.

V. ACKNOWLEDGEMENT

This work was sponsored by the Ministry of Higher Education under the Fundamental Research Grant Scheme (FRGS/1/2020/STG05/UTM/02/3). The authors were also greatly recognising the Universiti Teknologi Malaysia for the support in terms of equipment and facilities.

VI. DECLARATION OF FUNDING AND CONFLICTS OF INTEREST

The research leading to this paper's production was fully sponsored by the Ministry of Higher Education (Malaysia). This fund was awarded to A. Supee under the Fundamental Research Grant Scheme (FRGS) with the Grant Agreement No of FRGS/1/2020/STG05/UTM/02/3. For the non-financial interests, the authors have no conflicts of interest to declare that are relevant to the content of this paper. All of them have agreed to this paper submission.

VII. REFERENCES

Adusumilli, SP, Dederick, JM, Bae, IT, Garner, SM, Sharma, A, Westgate, CR & Dhakal, TP 2016, 'Iron pyrite thin films grown through a one-step annealing of iron oxide using sulfur sources, tert-butyl disulfide and H_2S', Thin Solid Films, vol. 615, pp. 271-280.

Aluri, V, Reddy, KTR & Reddy, YM 2015, 'Polycrystalline and single phase FeS_2 films grown by chemical bath deposition', Nanotechnology Reviews, vol. 4, no. 5, pp. 469-472.

Akhtar, MS, Alenad, A & Malik, MA 2015, 'Synthesis of mackinawite FeS thin films from acidic chemical baths', Materials Science in Semiconductor Processing, vol. 32, pp. 1-5.

Anuar, K, Tan, WT, Saravanan, N, Ho, SM & Gwee, SY 2009, 'Influence of pH values on chemical bath deposited FeS2 thin films', Pacific Journal of Science and Technology', vol. 10, pp. 801-805.

Axelevitch, A & Golan, G 2013, 'Hot-probe method for evaluation of majority charged carriers concentration in semiconductor thin films', Facta Universitatis, Series: Electronics and Energetics, vol. 26, no. 3, pp. 187-195.

Bhandari, KP, Roland, PJ, Koirala, P, Khanal, RR, Paudel, NR, Collins, R, Yan, Y, Heben, MJ & Ellingson, RJ 2015, 'Enhancing the efficiency of CdTe solar cells using a nanocrystalline iron pyrite film as an interface layer', IEEE 42nd Photovoltaic Specialist Conference (PVSC), New Orleans, 14-19 June 2015, pp. 1-4.

Bi, Y, Yuan, Y, Exstrom, CL, Darveau, SA & Huang, J 2011, 'Air stable, photosensitive, phase pure iron pyrite nanocrystal thin films for photovoltaic application', Nano Letters, vol. 11, no. 11, pp. 4953-4957.

Botchway, EA, Ampong, FK, Nkrumah, I, Boakye, FK & Nkum, RK 2019, 'Growth of a pure and single phase iron sulfide (pyrite) thin film by electrochemical deposition for photovoltaic applications', Open Journal of Applied Sciences, vol. 9, no. 9, pp. 725-735.

Ennaoui, A, Fiechter, S, Goslowsky, H & Tributsch, H 1985, 'Photoactive synthetic polycrystalline pyrite (FeS_2)', Journal of the Electrochemical Society, vol. 132, no. 7, pp. 1579-1582.

Ferrer, IJ, Nevskaia, DM, De las Heras, C & Sanchez, C 1990, 'About the band gap nature of FeS_2 as determined from optical and photoelectrochemical measurements', Solid State Communications, vol. 74, no. 9, pp. 913-916.

Henríquez, R, Vasquez, C, Briones, N, Munoz, E, Leyton, P & Dalchiele, EA 2016, 'Single phase FeS_2 (pyrite) thin films prepared by combined electrodeposition and hydrothermal low temperature techniques', International Journal of Electrochemical Science, vol. 11, pp. 4966-4978.

Hidzi, AH, Supee, A, Haladin, NB, Mohd Yusop, MZ & Wan Shamsuri, WN 2019, 'Role of tartaric acid on structural, morphological and optical properties of FeS_xO_y films formed by chemical bath deposition', Malaysian Journal of Chemistry, vol. 21, no. 3, pp. 110-116.

Hidzir, AH, Haladin, NB, Mohd Yusop, MZ, Ibrahim, N & Supee, A 2021, 'Influence of tartaric acid as the complexing agent on the properties of chemical bath deposited FeS_xO_y thin films', Materials Today: Proceedings, vol. 39, pp. 947-950.

Kawai, S, Yamazaki, R, Sobue, S, Okuno, E & Ichimura, M 2014, 'Electrochemical deposition of iron sulfide thin films and heterojunction diodes with zinc oxide', APL Materials, vol. 2, no. 3, pp. 032110.

Kassim, A, Soon, MH, Yean, YL, Wee, TT & Nagalingam, S 2012, 'Complexing agent effect on the properties of iron sulphide thin films', Canadian Journal of Applied Sciences, vol. 6, pp. 1863-1867.

Kassim, A, Wee, TT, Abdullah, DK, Sharif, AM, Soon, MH, Yong, GS & Nagalingam, S 2010, 'Preparation and characterization of iron sulphide thin films by chemical bath deposition method', Indonesian Journal of Chemistry, vol. 10, no. 1, pp. 8-11.

Kawai, S, Kajima, T & Ichimura, M 2016, 'Comparison of amorphous Fe–S–O and crystalline FeS_2 pyrite for photovoltaic application', Materials Research Express, vol. 3, no. 2, pp. 025901.

Kment, S, Kmentova, H, Sarkar, A, Soukup, RJ, Ianno, NJ, Sekora, D, Olejnicek, J, Ksirova, P, Krysa, J & Remes, Z 2014, 'Epoxy catalyzed sol–gel method for pinhole-free pyrite FeS_2 thin films', Journal of Alloys and Compounds, vol. 607, pp. 169-176.

La Notte, L, Salamandra, L, Zampetti, A, Brunetti, F, Brown, T, Di Carlo, A & Reale, A 2012, 'Airbrush spray coating of amorphous titanium dioxide for inverted polymer solar cells', International Journal of Photoenergy, vol. 2012, pp. 1-5.

Luo, L, Luan, W, Yuan, B, Zhang, C & Jin, L 2015, 'High efficient and stable solid solar cell: based on FeS_2 nanocrystals and P3HT: PCBM', Energy Procedia, vol. 75, pp. 2181-2186.

Manikandan, K, Mani, P, Dilip, CS, Valli, S, Inbaraj, PFH & Prince, JJ 2014, 'Effect of complexing agent TEA: The structural, morphological, topographical and optical properties of Fe_xS_x nano thin films deposited by SILAR technique', Applied Surface Science, vol. 288, pp. 76-82.

Morrish, R, Silverstein, R & Wolden, CA 2012, 'Synthesis of stoichiometric FeS_2 through plasma-assisted sulfurization of Fe_2O_3 nanorods', Journal of the American Chemical Society, vol. 134, no. 43, pp. 17854-17857.

Nakamura, S & Yamamoto, A 2001, 'Electrodeposition of pyrite (FeS_2) thin films for photovoltaic cells', Solar Energy Materials and Solar Cells, vol. 65, no. 1-4, pp 79-85.

Nie, X, Luo, S, Yang, M, Zeng, P, Qin, Z, Yu, W & Wan, Q 2019, 'Facile hydrothermal synthesis of nanocubic pyrite crystals using greigite Fe_3S_4 and thiourea as precursors', Minerals, vol. 9, no. 5, pp. 273 (1-13).

Orletskii, IG, Mar'yanchuk, PD, Maistruk, EV, Solovan, MN & Brus, VV 2016, 'Low-temperature spray-pyrolysis of FeS_2 films and their electrical and optical properties', Solid State Physics, vol. 58, no. 1, pp. 37-41.

Patterson, A L 1939, 'The Scherrer formula for X-ray particle size determination', Physical Review, vol. 56, no. 10, p. 978.

Prabukanthan, P, Thamaraiselvi, S & Harichandran, G 2017, 'Single step electrochemical deposition of p-type undoped and Co^{2+} doped FeS_2 thin films and performance in heterojunction solid solar cells', Journal of the Electrochemical Society, vol. 164, no. 9, pp. D581.

Qin, H, Jia, J, Lin, L, Ni, H, Wang, M & Meng, L 2018, 'Pyrite FeS_2 nanostructures: synthesis, properties and applications', Material Science and Engineering: B, vol. 236, pp. 104-124.

Rahman, MZ, Thyr, J & Edvinsson, T 2020, 'Surface polarity, water adhesion and wettability behaviors of iron pyrite', Materials Today: Proceedings, vol. 33, pp. 2465-2469.

Saragi, T, Permana, B, Saputri, M, Depi, BL, Butarbutar, SW, Safriani, L & Rahayu, I 2018, 'The effect of pH and sintering treatment on magnetic nanoparticles ferrite based synthesized by coprecipitation method', Journal of Physics: Conference Series, vol. 1080, pp. 012019.

Srivastava, RP & Ingole, S 2020, 'An investigation on the phase purity of iron pyrite (FeS_2) thin films obtained from the sulfurization of hematite (Fe_2O_3) thin films', Materials Science in Semiconductor Processing, vol. 106, pp. 104775.

Srivastava, RP, Saxena, A & Ingole, S 2017, 'n-type iron pyrite (FeS_2) thin-films obtained at different sulfur vapor pressures', Chalcogenide Letters, vol. 14, no. 6, pp. 227-237.

Supee, A & Ichimura, M 2016, 'Effects of complexing agents on electrochemical deposition of FeS_xO_y thin films', Japanese Journal of Applied Physics, vol. 55, no. 8, pp. 081202.

Supee, A & Ichimura, M 2017, 'Effects of complexing agents on electrochemical deposition of FeS_xO_y in ZnO/FeS_xO_y heterostructures', Applied Physics A, vol. 123, no. 12, pp. 1-3.

Thibeau, RJ, Brown, CW & Heidersbach, RH 1978, 'Raman spectra of possible corrosion products of iron', Applied Spectroscopy, vol. 32, no. 6, pp. 532-535.

Umehara, M, Takeda, Y, Azuma, H & Motohiro, T 2012, 'Laser annealing to form high-temperature phase of FeS_2', Japanese Journal of Applied Physics, vol. 51, no. 2S, pp. 02BP10.

Vedavathi, A, Munikrishna, Y & Ramakrishna, K 2015, 'Role of ammonia on structural, electrical, FTIR and optical studies of FeS_2 films formed by CBD', IOSR Journal of Engineering vol. 5, no. 2, pp. 65-70.

Walter, J, Zhang, X, Voigt, B, Hool, R, Manno, M, Mork, F, Aydil, ES & Leighton, C 2017, 'Surface conduction in n-type pyrite FeS_2 single crystals', Physical Review Materials, vol. 1, no. 6, pp. 065403.

Wang, DY, Jiang, YT, Lin, CC, Li, SS, Wang, YT, Chen, CC & Chen, CW 2012, 'Solution-processable pyrite FeS_2 nanocrystals for the fabrication of heterojunction photodiodes with visible to NIR photodetection', Advanced Materials, vol. 24, no. 25, pp. 3415-3420.

Wu, P, Zhou, C, Li, Y, Zhang, M, Tao, P, Liu, Q & Cui, W 2021, 'Flower-like FeOOH hybridized with carbon quantum dots for efficient photo-Fenton degradation of organic pollutants', Applied Surface Science, vol. 540, no. 2, pp. 148362.

Zhang, H, Bayne, M, Fernando, S, Legg, B, Zhu, M, Penn, RL & Banfield, JF 2011, 'Size-dependent bandgap of nanogoethite', The Journal of Physical Chemistry C, vol. 115, no. 36, pp. 17704-17710.